Reentrant spin glass state in the long-range magnetic order compound Er_2Cu_2In

Baidyanath Sahu,[1,2] Ramesh Kumar,[2,3] R. Djoumessi Fobasso,[2] Rishabh Shukla,[4,*] Sindisiwe P. Xhakaza,[2] and André M. Strydom[2]

[1]*Department of Chemistry, Indian Institute of Technology Bombay, Mumbai 400076, India*

[2]*Highly Correlated Matter Research Group, Department of Physics, University of Johannesburg, P.O. Box 524, Auckland Park 2006, South Africa*

[3]*Department of Electronics Physics, GITAM Institute of Science, GITAM Deemed to be University, Rushikonda, Visakhapatnam, Andhra Pradesh 530045, India*

[4]*Laboratory for High-Performance Ceramics, Swiss Federal Laboratories for Materials Science and Technology (Empa), Überlandstrasse 129, 8600 Dübendorf, Switzerland*

(Received 8 June 2025; revised 12 February 2026; accepted 10 March 2026; published 3 April 2026)

We have investigated the structural, magnetic, and transport characteristics of single-phase polycrystalline Er_2Cu_2In. Er_2Cu_2In adopts a tetragonal structure reminiscent of Mo_2B_2Fe-type, with a space group of $P4/mbm$ (No. 127). Below a critical temperature (T_C) of 41 K, we have confirmed long-range ferromagnetic (FM) ordering through dc magnetization, specific heat capacity, and electrical resistivity. The temperature-dependent ac-magnetic susceptibility under varying excitation frequencies and ac-driven fields has shown the existence of a spin glass state below the FM transition temperature. We have employed a combination of methods, including Vogel-Fulcher, Arrhenius activation, and critical-scaling approaches, to analyze the ac-magnetic susceptibility data and estimate the dynamical parameters governing spin dynamics in Er_2Cu_2In. Furthermore, the magnetoresistance exhibits significant variations around the FM transition temperature, indicative of the rich and intricate magnetic behavior inherent to Er_2Cu_2In.

DOI: 10.1103/jqs4-hg41

I. INTRODUCTION

Over the last few decades, research into the spin glass state of magnetic systems has been pursued as an interesting mechanism, particularly in rare-earth-based materials, where spin magnetic entropy may be realized as an alternative to long-range magnetic order and collective behavior towards the ground state at low temperatures. The spin glass state is often observed in geometric or magnetically frustrated systems. Crystallographically well-ordered compounds can also exhibit spin glass behavior [1–4]. The crystal electric field (CEF) plays an important role in well-ordered compounds for the spin glass behavior due to dynamic fluctuations of magnetic moments, resulting in a frustrated magnetic ground state [5–8]. Many types of magnetic frustration systems have been investigated in the literature, and among them, the Shastry-Sutherland lattice is one of the simplest frustrated systems. Here, the relative strength of interdimer coupling (J) and intradimer coupling (J') plays supplementary roles leading to spin frustration [9–11]. It has also been reported that the atomic arrangement of the R_2T_2X (R = rare earths, T = transition metals, X = *s*- and *p*-block elements) series of compounds with tetragonal structure follows the Shastry-Sutherland lattice configuration [12–18].

The family of R_2T_2X compounds in the Mo_2B_2Fe type tetragonal structure with space group $P4/mbm$ (No. 127) has garnered significant attention for their large variation in magnetic properties at low temperatures, including magnetic ordering, magnetic frustration, spin glass anomalies, and large magnetocaloric effects. In R_2T_2X compounds, R atoms occupy one single site in the crystal structure and form dimers in the basal plane. Therefore, the coordination environment of the R atoms in R_2T_2X compounds gives rise to a complex network of magnetic interactions, resulting in a diverse and rich phase diagram. Notably, these compounds feature magnetic dimers formed by pairs of rare-earth atoms [12–26]. The dimers are often coupled via antiferromagnetic interactions, resulting in an overall magnetic ground state with a net magnetic moment. Despite extensive studies on the magnetocaloric aspects of R_2T_2X systems, the coexistence of long-range magnetic ordering and spin glass anomalies due to competition among exchange interaction strength (J), crystalline electric field, and magnetic frustration has not received sufficient attention.

F. M. Schappacher *et al.* [22] and I. P. Fisher *et al.* [23] reported low-temperature ferromagnetic behavior in R_2Cu_2Cd (T_C = 14.5–86.2 K) and R_2Cu_2In (T_C = 26.7–85.5 K). The dc- and ac-magnetic studies of Gd_2Cu_2Cd (T_C = 110 K) and Tm_2Cu_2In (T_C = 32.5 K) exhibit spin glass behavior below their magnetic transition temperature. G. Sala *et al.* [26] investigated the magnetic properties of Nd_2Ni_2In through inelastic neutron scattering and reported the existence

*Contact author: rishabh.shukla@empa.ch

Published by the American Physical Society under the terms of the Creative Commons Attribution 4.0 International license. Further distribution of this work must maintain attribution to the author(s) and the published article's title, journal citation, and DOI.

of Ising antiferromagnetism with a large moment in the geometrically frustrated Shastry-Sutherland lattice. Another Shastry-Sutherland single crystal of Tb_2Pd_2In exhibits a collinear structure of rare-earth cations with long-wavelength periodicity. P. Král *et al.* [16] provided a detailed investigation of the magnetic and lattice properties of Tm_2Cu_2In under elevated pressures, shedding light on the complex behavior of this intermetallic compound.

This article explores the physical properties of the single-phase polycrystalline intermetallic compound Er_2Cu_2In, synthesized by the arc-melting process. We systematically studied temperature and field-dependent dc- and ac-magnetic properties, specific heat capacity, and electrical resistivity. The obtained spin glass state is illustrated by magnetic characterizations. The large field dependence of magnetoresistance in Er_2Cu_2In has been observed.

II. EXPERIMENTAL DETAILS

Polycrystalline Er_2Cu_2In was synthesized using a high-purity (99.9 wt%) elemental mixture in a stoichiometric ratio. The mix of elements was melted under an argon atmosphere using an Edmund Bühler (GmbH) arc-melting furnace. To ensure homogeneity, the resulting ingot was flipped and remelted multiple times. Subsequently, the ingot was carefully wrapped in tantalum foil, sealed in a quartz tube under a high vacuum (in the order of 10^{-6} bar), and subjected to heat treatment at 973 K for one week. After the heat treatment, the sample was rapidly quenched in water. Structural analysis of the synthesized material was performed using powder x-ray diffraction (XRD) with a Rigaku x-ray diffractometer utilizing CuK_α radiation. The obtained powder diffraction pattern was further analyzed using the Rietveld refinement with FullProf software [27,28] for phase analysis and to determine the structural parameters. Temperature- and magnetic-field-dependent magnetization measurements were conducted using a commercial DynaCool Physical Properties Measurement System (PPMS) (Quantum-Design, San Diego, USA). To avoid the field-cycling effect between two isothermal magnetizations, the sample was heated to 100 K (above the Curie temperature) after each isotherm was measured. The temperature dependence of magnetization was recorded using the zero-field-cooled (ZFC) and field-cooled (FC) protocols in the temperature range of 2 to 300 K and up to a field of 0.75 T. In the ZFC protocol, the sample was cooled from 300 to 2 K in zero magnetic field, and the magnetization was recorded as it warmed after applying a constant magnetic field. In the FC protocol, the sample was cooled from 300 to 2 K under the same applied magnetic field, and the magnetization was recorded as it warmed. The temperature dependence of ac-susceptibility measurements was performed using the ACMS option of the PPMS DynaCool with a frequency range of 300 to 9000 Hz. An ac-driven field of 0.3 mT was employed for the temperature variation of ac susceptibility for different frequencies. Additionally, the temperature dependence of ac-susceptibility measurements was conducted by varying the ac-driven field from 0.3 to 1.5 mT at a frequency of 1000 Hz. The specific heat capacity was measured under quasiadiabatic conditions using the heat capacity option of the PPMS DynaCool. Four-probe electrical resistivity and magnetoresistance (MR) measurements were also performed using the same PPMS DynaCool in the temperature range from 2 to 300 K and up to a magnetic field of 9 T.

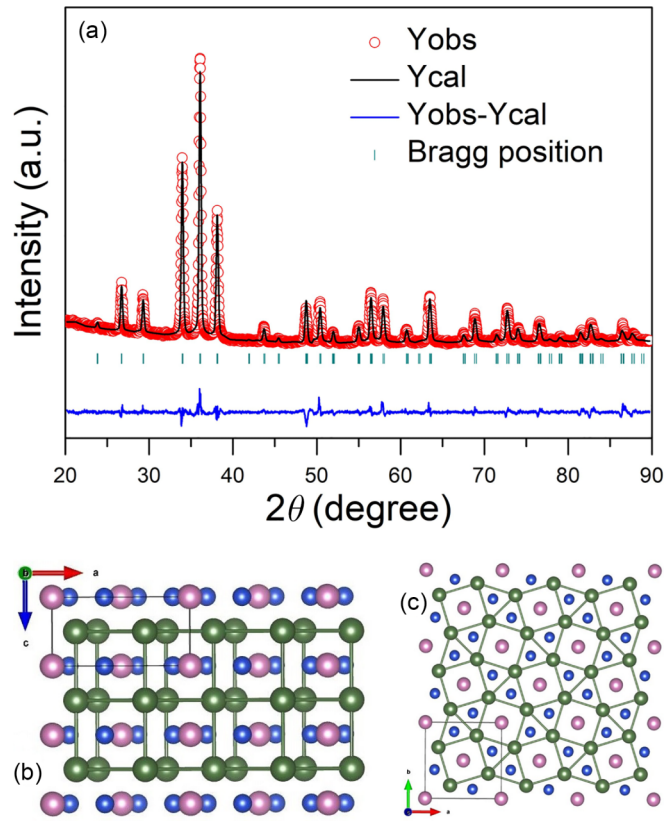


FIG. 1. (a) Rietveld refinement of recorded powder x-ray diffraction pattern of Er_2Cu_2In. Schematic structure of Er_2Cu_2In (b) along the *b* axis showing the layered atomic arrangement, and (c) in the *ab* plane mimics the two-dimensional Shastry-Sutherland atomic arrangement in the isosceles triangular and square lattice pattern. Er, Cu, and In atoms are presented as green, blue, and pink solid spheres, respectively.

III. RESULTS AND DISCUSSION

A. X-ray diffraction

The Rietveld refined room temperature powder x-ray diffraction pattern of Er_2Cu_2In is displayed in Fig. 1(a). The Rietveld refinement reveals that the Er_2Cu_2In crystallizes in a single-phase tetragonal structure with space group $P4/mbm$ (No. 127). The Rietveld-refined lattice parameters are summarized in Table I and are in good agreement with the previous Refs. [23,29]. Further, Figs. 1(b) and 1(c) show the schematic atomic arrangement of Er_2Cu_2In in a tetragonal structure generated from the Rietveld refined data using the Vesta software [30]. Figure 1(b) shows the atomic layer arrangements of Er_2Cu_2In along the *b* axis where $4f$–Er atoms occupy one layer, and Cu and In atoms are arranged in another layer of the same crystal structure. Also, the Er atoms simultaneously form a special isosceles triangular and square lattice arrangement in the *ab* plane shown in the Fig. 1(c), which is equivalent to the two-dimensional Shastry-Sutherland lattice [18]. Moreover, the shortest Er–Er bond lengths in Er_2Cu_2In

TABLE I. The lattice parameters and unit cell volume of Er_2Cu_2In obtained from the Rietveld refinement of XRD pattern for the tetragonal phase ($P4/mbm$, No. 127), along with atomic coordinates.

a	7.463(2) Å
b	7.463(2) Å
c	3.736(1) Å
V	208.076(2) Å^3
R_p	17.9
R_{wp}	14.6
$R_{\exp}$	4.8

Atomic coordinates for Er_2Cu_2In

Atom	Wyckoff	x	y	z
Er	4g	0.1724(2)	0.6724(2)	0.5
Cu	4h	0.6226(1)	0.1226(1)	0.0
In	2a	0.0	0.0	0.0

are 3.582 and 3.872 Å, which suggests that the coupling between the Er atoms is governed by the two exchange integrals (J) corresponding to these bond lengths in the crystal structure. Therefore, we further investigate the magnetic properties of Er_2Cu_2In in detail.

B. dc-magnetic properties

The temperature dependence of dc-magnetic susceptibility measured under an applied magnetic field of 0.01 T is shown on the left axis of Fig. 2 (solid blue circles) and exhibits a paramagnetic (PM) to ferromagnetic (FM) phase transition. The first-order derivative of the dc-magnetic susceptibility, i.e., $d\chi(T)/dT$, is presented in the upper left inset (a) of Fig. 2 and provides the Curie temperature of $T_C = 41$ K. The obtained T_C value is in good agreement with the previous reports [23,29]. The inverse of $\chi(T)$ is presented on the right axis of Fig. 2, revealing that the $\chi^{-1}(T)$ curve exhibits a linear paramagnetic behavior for T > 100 K. Consequently, a linear fit (T > 100 K) using the Curie-Weiss law $\chi = C/(T - \theta_p)$, (where C is the Curie-Weiss constant and θ_p is the Curie-Weiss temperature), yields C = 23.48 K-emu-mol^{-1}Oe^{-1} and $\theta_p = 16.1$ K. The positive value of θ_p indicates a predominant ferromagnetic exchange interaction in Er_2Cu_2In. The calculated effective magnetic moment (μ_{eff}) is found to be 9.69 μ_B/Er^{3+} ion, which is close to the theoretical free magnetic moment of Er^{3+} [$g\sqrt{J(J+1)}$] = 9.58 μ_B]. This result indicates that the localized 4f shells of Er^{3+} contribute to the magnetic properties.

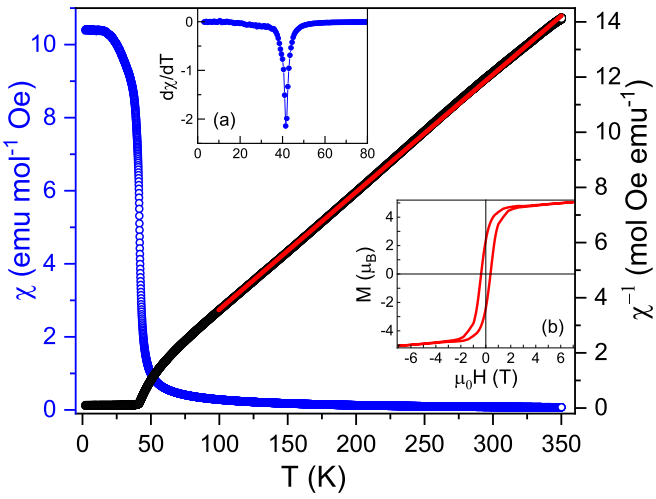


FIG. 2. Left axis: Temperature dependence of dc-magnetic susceptibility [$\chi(T)$] of Er_2Cu_2In measured under an external field of a 0.01 T. Right axis: temperature variation of reciprocal dc-magnetic susceptibility $\chi^{-1}(T)$ with a Curie-Weiss fit shown as a red solid line on the experimental data. Inset (a) represents the $d\chi(T)/dT$, inset (b) is the field-dependent magnetization (M-H) loop at 2 K.

The applied magnetic field dependence of the isothermal magnetization (M-H) loop at 2 K is recorded within the ± 7 T and is presented in the bottom right inset (b) of Fig. 2. Here, one can see that the M-H loop exhibits a well-defined hysteresis loop with finite magnetic remanence and coercivity values of 4.7 μ_B and 0.4 T, respectively, which are characteristic of ferromagnetic materials. It is also noted that the field dependence of magnetization does not saturate even at the high magnetic fields of $\mu_0 H = 7$ T. The obtained magnetic moment of 5.05 μ_B/Er^{3+} at 7 T appears to be ≈56% of the saturation moment value expected for parallel alignment of Er^{3+} (gJ = 9 μ_B, with g = 6/5, J = 15/2) moments. This reduction of saturation magnetization may be attributed to the influence of anisotropy due to the crystal electric field and/or the frustrated magnetic moments in the system [31]. Isothermal magnetization at different temperatures was recorded to find the order of magnetic phase transitions in Er_2Cu_2In. No significant changes in the magnetization are observed over the temperature range from 2 to 30 K (not shown in the figure). However, the magnetization above 30 K gradually decreases with increasing temperature due to thermal agitation in the spin lattice. This suggests that Er_2Cu_2In might exhibit complex magnetic phenomena at low temperatures.

The field dependence of magnetization demonstrates a sigmoidal-type variation with a tendency to saturate at low fields. At high magnetic fields, the linear variation of the magnetization suggests the presence of magnetic anisotropy and crystal field effects. Notably, the inverse susceptibility deviates from the expected Curie-Weiss behavior at low temperatures (below 100 K), indicating a strong presence of magnetocrystalline anisotropy in the system. This observation is further supported by the estimation of saturation magnetization, which was found to be 5.05 μ_B/Er^{3+} at 7 T. In Er_2Cu_2In, the Er ion is at the orthorhombic point symmetry with C_{2v} symmetry. The ground state multiplet $^4I_{15/2}$ ($J = \frac{15}{2}$, $L = 6$, $S = \frac{3}{2}$) of the 4f orbital of the Er^{3+} ion splits into eight doublets due to the crystal field effect (CEF). The CEF Hamiltonian ($\mathcal{H}_{\text{CEF}}$) for such a case can be expressed as

$$\mathcal{H}_{\text{CEF}} = B_2^0 O_2^0 + B_2^2 O_2^2 + B_4^0 O_4^0 + B_4^2 O_4^2 + B_4^4 O_4^4 + B_6^0 O_6^0 + B_6^2 O_6^2 + B_6^4 O_6^4 + B_6^6 O_6^6, \quad (1)$$

where B_n^m are the crystal field parameters, and O_n^m are the Stevens operators. The Stevens operators are defined as

$$O_n^m = \sum_{\mu,\nu} (2J+1)\langle J\mu|O_n^m|J\nu\rangle |J\mu\rangle\langle J\nu|, \quad (2)$$

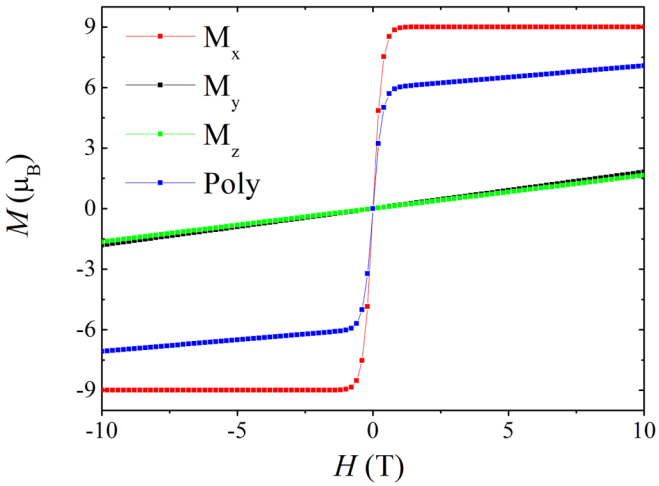


FIG. 3. Simulated field dependence of magnetization along three different axes (M_x, M_y, and M_z) and the polycrystalline average for Er_2Cu_2In. The M_x moment is fully saturated, indicating easy alignment along the x axis. The M_z moment shows a linear variation, suggesting that the z axis is the hard axis requiring a higher field strength for alignment.

where $|J\mu\rangle$ and $|J\nu\rangle$ are the eigenstates of the total angular momentum operator J.

The PyCrystalField code [32] utilizes the crystal field Hamiltonian expressed in terms of the CEF parameters and Stevens operators to simulate the magnetization and susceptibility of Er_2Cu_2In. By providing the Crystallographic Information File (CIF) containing the crystal structure information of Er_2Cu_2In, the PyCrystalField code can extract the necessary crystal field parameters and perform calculations based on the defined Hamiltonian. This allows for the simulation of magnetization and susceptibility of Er_2Cu_2In at various temperatures and magnetic fields. Figure 3 illustrates the field dependence of magnetization along three different axes and their polycrystalline average, providing insights into the magnetic behavior of Er_2Cu_2In. The moment along the x axis (M_x) is fully saturated, indicating effortless alignment along the x axis. In contrast, the M_z moment shows a linear variation, suggesting the z axis is the hard axis, requiring a higher field strength for alignment. The polycrystalline average reveals a reduced magnetic moment and exhibits a linear variation at high field strengths. These findings align with the experimental observation of a low saturation moment, indicating the influence of easy and hard axes on the magnetic behavior of Er_2Cu_2In. The results presented in Fig. 3 contribute valuable insights into the magnetic properties of Er_2Cu_2In, supporting the conclusion that the magnetic moments' easy axis is perpendicular to the c axis. Furthermore, the Er_2Cu_2In compound exhibits complex magnetic behavior attributed to competing interactions between different magnetic moments that lead to geometric frustration. This frustration arises from the compound's crystal structure, which can lead to degenerate or nearly degenerate ground states, resulting in a diverse range of magnetic behaviors.

As we discussed earlier, the compound Er_2Cu_2In crystallizes in the tetragonal space group $P4/mbm$ (No. 127). The Er atoms form a layered network in the ab plane that repeats along the c axis. Within this structure, three short Er–Er distances define the main magnetic interactions. The shortest bond (3.582 Å) lies in the ab plane along the (110) diagonal. The next bond (3.723 Å) connects Er atoms vertically along the c axis. The third bond (3.872 Å) links four neighboring Er atoms in the plane at different angles with respect to the a axis. In a conventional magnetic dimer system, two neighboring spins are connected by a strong AFM interaction, which is stronger than all other interactions in the lattice. This strong AFM interaction leads to local spin singlets and a nonmagnetic ground state with a spin gap. For example, in Shastry-Sutherland or spin ladder systems, the ratio of the nearest-neighbor J_1 to the next-nearest-neighbor J_2 lies between 0.5 and 0.7, stabilizing isolated dimers. In Er_2Cu_2In, the complex anisotropic exchange interaction departs from this simple dimer picture. Figure S1(a) [33] shows the magnetic exchange constant as a function of scaled distance. The first-neighbor J_1 interaction is predominantly ferromagnetic (0.65 meV) with negligible Dzyaloshinskii-Moriya (DM) interaction (see Fig. S1(b–d) [33]). The J_3 shell contains multiple inequivalent bonds with mixed signs in the ab plane. The strongest interaction is AFM at -3.05 meV, while others are weakly FM. Notably, the antisymmetric D value is significant for this interaction. These AFM interactions could, in principle, favor dimer formation; however, mixed AFM and FM interactions, as well as strong DM interactions, would prevent dimer formation. Therefore, Er_2Cu_2In cannot be regarded as a canonical dimer system. The nearest-neighbor and interlayer exchange interactions in Er_2Cu_2In are predominantly ferromagnetic rather than antiferromagnetic; hence, the system can be classified as a frustrated anisotropy magnetic network. The competition between FM/AFM and a sizable DM interaction stabilizes a noncollinear spin arrangement.

C. Specific heat capacity

Figure 4(a) shows the heat capacity measured in the absence of an external magnetic field for Er_2Cu_2In, along with the isostructural nonmagnetic compound Y_2Cu_2In. At room temperature (300 K), the heat capacity attains a value of nearly 128 and 124 J mol^{-1} K^{-1} for Er_2Cu_2In and Y_2Cu_2In, which is very close to the Dulong-Petit limit of $3nR = 124.7$ J mol^{-1}K^{-1}, where $n = 5$ is the number of atoms per formula unit, and R stands for the gas constant. A pronounced λ–shape anomaly around the magnetic transition temperature confirms long-range magnetic ordering in Er_2Cu_2In. The magnetic contribution to the heat capacity (C_{4f}) is estimated by subtracting the isostructural nonmagnetic Y_2Cu_2In. The temperature dependence of C_{4f} is shown in the inset of Fig. 4(a) with solid blue circles. However, C_p (solid black squares) closely overlap at higher temperatures for both Y_2Cu_2In and Er_2Cu_2In.

Figure 4(b) presents the C_p data measured under various magnetic fields from 0 to 9 T in the temperature range of 70 to 2 K. As seen in Fig. 4(b), the C_p data for all fields show only one anomaly around the transition temperature. It is also evident from Fig. 4(b) that the peak associated with the phase transition becomes broader and shifts towards higher temperatures as the applied magnetic field increases. This result confirms that C_p at different fields exhibits

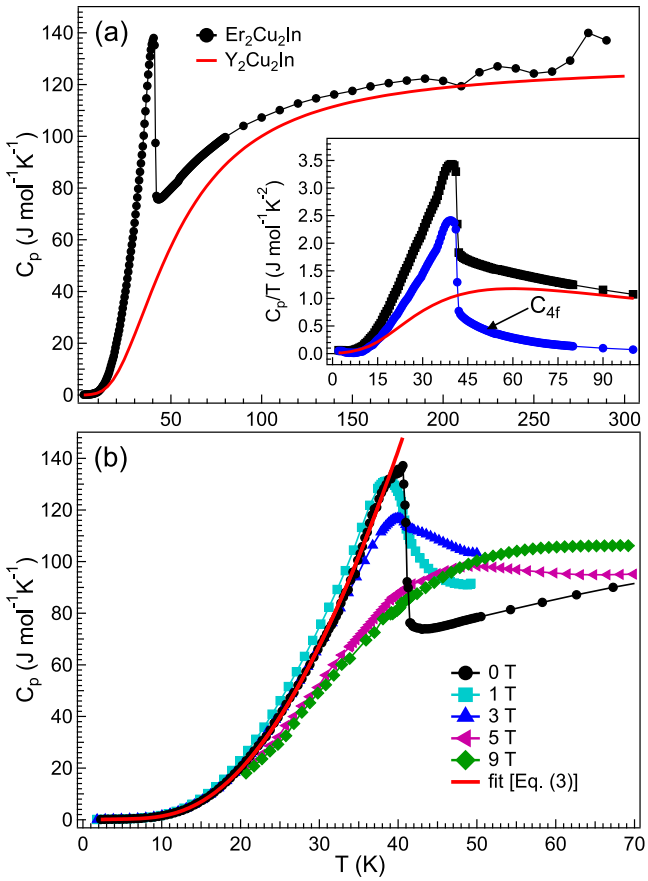


FIG. 4. (a) Temperature variations of heat capacity C_p of Er_2Cu_2In (solid black circles) and Y_2Cu_2In (solid red line) measured in zero-magnetic field. The inset shows the temperature variations of C_p/T, where the blue solid circles curve shows $4f$–electron contribution to the heat capacity of Er_2Cu_2In. (b) Low temperature C_p measured in different magnetic fields. The solid line is the least squares (LSQ) fit of Eq. (3) to the experimental data at 0 T.

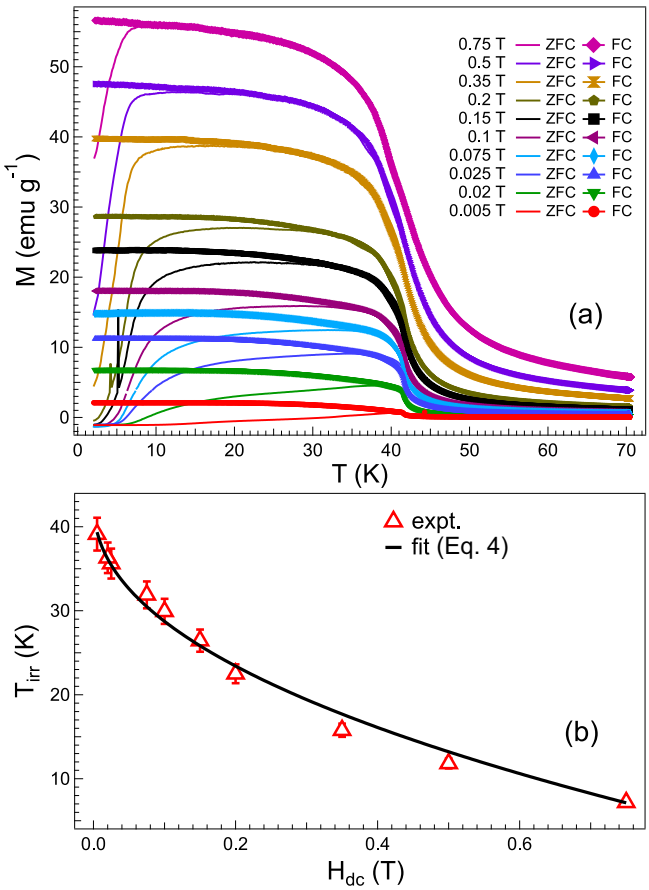


FIG. 5. (a) Temperature-dependent ZFC and FC magnetization measured under various applied magnetic fields, and (b) a power-law fit of the irreversibility (T_{irr}) temperature (T_{irr} is the bifurcation temperature between ZFC and FC magnetization) with the different dc-applied magnetic fields.

ferromagnetic characteristics for Er_2Cu_2In. However, a slight downward shift for $\mu_0 H = 1$ T shows antiferromagnetic behavior. This feature is commonly observed in ferromagnetic compounds at low applied magnetic fields due to the delicate balance between competing exchange and magnetocrystalline interactions in the zero-field ordered phase [34]. The change in C_p (ΔC_p) of a ferromagnetic material is dominated by the magnon contribution below T_C. The heat capacity (C_p) in the magnetic ordering region of ferromagnetic material depends upon $T^{3/2}$. Below T_C, the C_p data can be described by the spin excitation formula [35]:

$$C_p(T) = \gamma_e T + BT^{3/2} \exp\left(\frac{-\Delta}{T}\right), \tag{3}$$

where γ_e is the electronic contribution to the heat capacity in the ordered state, and $BT^{3/2}\ \exp\left(\frac{-\Delta}{T}\right)$ represents the magnon contribution characterized by an energy gap Δ in the ferromagnetic spin wave spectrum. Below the magnetic transition, LSQ fits of Eq. (3) to the C_p data are shown in Fig. 4(b) as a red solid line. The fitting parameters yielded are $\gamma_e = 0.047 \pm 0.008$ J mol^{-1}K^{-1}, B $= 1.493 \pm 0.024$ J mol^{-1}K^{-1} and $\Delta = 39.4 \pm 0.5$ K. The obtained value of Δ, which is quite close to the value of T_C, provides confidence for the use of the above expression for describing the zero-field data of C_p below T_C [36].

D. Spin glass behavior

Figure 5(a) displays the ZFC and FC temperature dependence of dc magnetization of Er_2Cu_2In under various applied magnetic fields ranging from $\mu_0 H = 0.005$ to 0.75 T. As shown in Fig. 5(a), the FC magnetization exhibits ferromagnetic features for all magnetic field values. However, the ZFC magnetization increases sharply with temperature and shows distinct plateau behavior in the temperature range from ∼7 to 40 K. It is also observed from Fig. 5(a) that the ZFC and FC magnetization curves demonstrate magnetic thermodynamic irreversibility below T_C. The reduction of ZFC magnetization with decreasing temperature leads to this irreversibility. Additionally, it is observed that the irreversibility temperature, T_{irr}, is strongly dependent on the applied magnetic field, consistent with the SG transition, suggesting that the ferromagnetic compound possesses reentrant spin glass properties [1]. Therefore, a H-T phase diagram with the applied dc-applied magnetic field (H_{dc}) and T_{irr} is plotted in Fig. 5(b) where T_{irr} decreases with increasing H_{dc}. The H-T phase diagram of spin

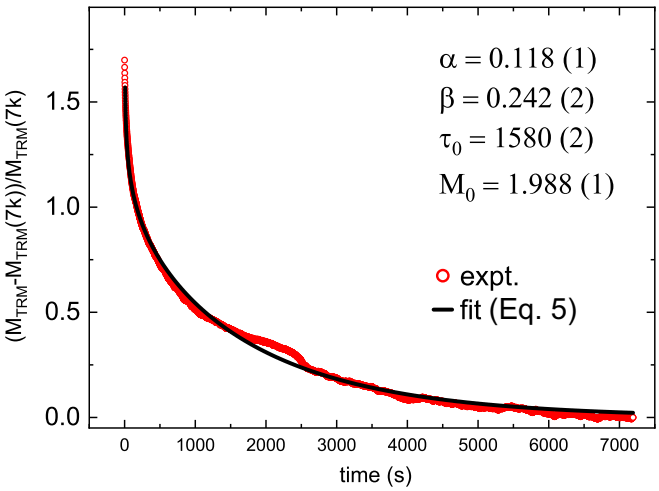


FIG. 6. Time-dependent decay of thermoremanent magnetization (TRM) in Er_2Cu_2In. The normalized magnetization ($\bar{M}$) is plotted as a function of time (τ) and fitted using a stretched exponential function given by Eq. (5).

glasses generally follows either an Almeida-Thouless (AT) line ($T \propto H^{2/3}$) or a Gabay-Thoulouse line ($T \propto H^2$), which are linked to Ising spin glasses or strong anisotropic systems, and Heisenberg or weakly anisotropic systems, respectively. However, a deviation from these two models is evaluated through the general equation [37],

$$T_{irr}(H_{dc}) = T_0^{irr}\left(1 - A_{irr}H_{dc}^{2/\Phi_{irr}}\right), \tag{4}$$

where T_0^{irr}, A_{irr}, and Φ_{irr} are the T_{irr} in the limit of zero dc-magnetic field, amplitude for irreversibility temperature, and crossover component related to the dependence of T_{irr} on H_{dc}, respectively. Therefore, to evaluate this H-T phase diagram in Er_2Cu_2In, Eq. (4) is used to fit the experimental data in Fig. 5(b) and yields $T_0^{irr} = 42.97 \pm 1.75$, $A_{irr} = 0.952 \pm 0.024$, and $\Phi_{irr} = 4.59 \pm 0.45$. Here, the value of Φ_{irr} is larger than the AT/GT line ($\Phi = 3$ or 2) and diverges from these models [4,37] showing the dominant anisotropy in Er_2Cu_2In. Similar values of Φ_{irr} are obtained in the Refs. [38–41] (discussed below).

A time-dependent measurement of thermoremanent magnetization (TRM) was conducted to understand the spin dynamics of Er_2Cu_2In. The sample was cooled from a temperature well above T_C to the measuring temperature (T_m) under an applied dc-magnetic field of 200 Oe. Once T_m was reached, the field was turned off, and after a waiting period of 4 hours, the field was reapplied, and the dc magnetization was recorded. It was found that the time-dependent decay of M_{TRM} in Fig. 6 fits well (solid black line) with the stretched exponential function over the entire time interval given below [42],

$$\bar{M} = M_0\tau^{-\alpha}\exp[(-\tau/\tau_0)^{\beta}], \tag{5}$$

where $\bar{M}$ is the normalized magnetization, M_0 is the longitudinal spontaneous magnetization coexisting with the frozen transverse spin component, and α, τ_0, and β are the exponents that can be extracted from the nonlinear fitting. The fitting parameters align with those found in some metallic glasses with large random magnetic anisotropy [42]. The time-dependent decay of the thermoremanent magnetization (TRM) in Er_2Cu_2In follows a stretched exponential function in Fig. 6, as described by Eq. (5). The fitting parameters obtained from the analysis include $M_0 = 1.988 \pm 0.001$, $\alpha = 0.118 \pm 0.001$, $\tau_0 = 1580 \pm 2$, and $\beta = 0.242 \pm 0.002$. These values suggest that Er_2Cu_2In exhibits behavior similar to bulk metallic glasses with random magnetic anisotropy and Ising spins. The presence of stretched exponential decay indicates complex spin dynamics and relaxation processes in Er_2Cu_2In. The parameters α, τ_0, and β reflect the interplay between spin interactions, magnetic anisotropy, and energy barriers in determining the magnetic behavior of Er_2Cu_2In. This highlights the unique magnetic properties of Er_2Cu_2In and its resemblance to other systems with random magnetic anisotropy.

To investigate the possibility of a spin glass state, we performed temperature-dependent ac-susceptibility measurements at different excitation frequencies (300–9000 Hz) and various amplitudes of an ac-driven field (0.3–1.5 mT). Figure 7(a) shows the real/in-phase component, $\chi'(f, T)$, of the ac susceptibility versus temperature for Er_2Cu_2In in the frequency range from 300 to 9000 Hz, while the ac-driven field was 0.3 mT. As shown in Fig. 7(a), the $\chi'(T)$ data exhibit a peak near T_C. The curves show maxima whose amplitudes and positions vary with the excitation frequency. It can also be seen from Fig. 7(a) that the peak position shifts toward higher temperatures (highlighted with a solid black arrow), and the peak amplitude decreases with increasing frequency (highlighted in the inset of Fig. 7(a) with a solid downward arrow). These features are commonly observed in spin glass systems due to geometric and magnetic frustration. The imaginary part of the temperature variation $\chi'(f, T)$ shown in Fig. 7(b) also indicates that the peak position shifts with the excitation frequencies from 39.7 to 40.5 K, which is highlighted using a solid downward black arrow. However, the change of $\chi'(f, T)$ in terms of amplitude and peak positions with excitation frequencies is significantly smaller as compared to $\chi''(f, T)$. Figures 7(c) and 7(d) display the real, $\chi'(H_{ac}, T)$, and imaginary, $\chi''(H_{ac}, T)$, components of the ac susceptibility measured under different ac-driven magnetic field ranges from 0.3 to 1.5 mT with a fixed excitation frequency of 1000 Hz. As seen in Fig. 7(c), peak positions of $\chi'(H_{ac}, T)$, slightly shift with the ac-driven magnetic field, which is highlighted with a solid black arrow, and the decrease in amplitude with decreasing ac-driven magnetic field is highlighted in the inset of Fig. 7(c) using a solid downward black arrow. From Fig. 7(d), it is evident that as the ac-driven field decreases, the magnitude of $\chi''(H_{ac}, T)$ peak is significantly suppressed and shifts to higher temperatures from 38.4 to 40.1 K when changing the field from 1.5 to 0.3 mT, respectively. Similar to Figs. 7(a) and 7(b), the change of $\chi'(H_{ac}, T)$ in terms of amplitude and peak positions with ac-driven field is significantly smaller as compared to $\chi''(H_{ac}, T)$. These features generally indicate the coexistence of a spin glass material. These observed results indicate that Er_2Cu_2In displays ferromagnetic behavior with spin glass anomalies.

To further quantitatively investigate the glassy spin state in Er_2Cu_2In, we further analyze the experimental real/in-phase component (χ') and imaginary/out-of-phase component (χ'')

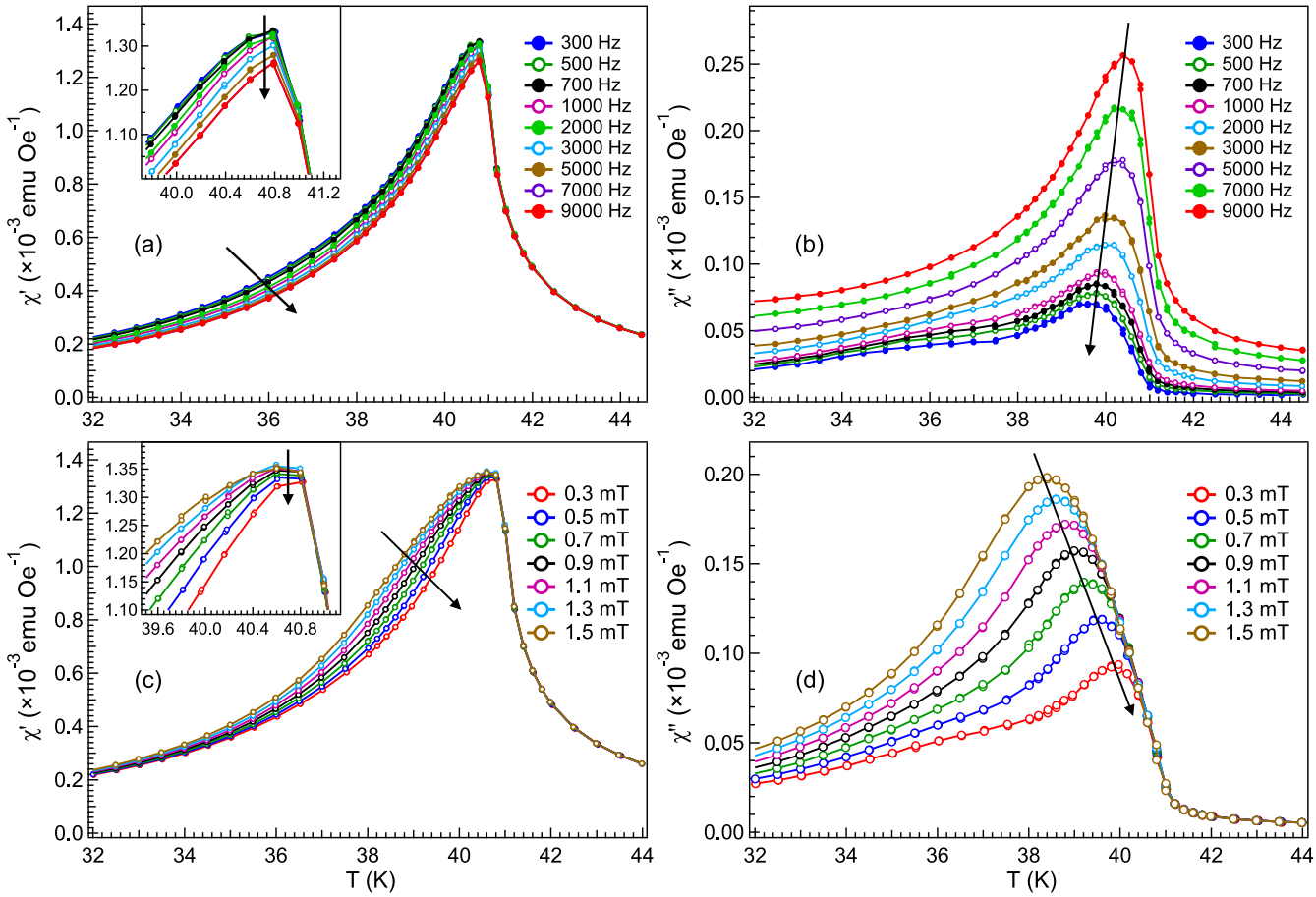


FIG. 7. Temperature-dependent ac-magnetic susceptibility at different excitation frequencies between 300 and 9000 Hz at a constant ac-driven field of 0.3 mT, (a) real/in-phase χ' (f, T) component (solid black arrow points toward the variation with the excitation frequencies), inset shows the variation of amplitude with excitation frequencies using a solid downward black arrow, and (b) imaginary/out-of-phase χ'' (f, T) component (solid downward black arrow points toward the peak shift with excitation frequency). Temperature-dependent ac-magnetic susceptibility in different ac-driven fields with a constant excitation frequency of 1000 Hz (solid arrow points toward the variation with excitation frequency), inset shows the variation of amplitude with excitation frequency using a solid black arrow, (c) real/in-phase χ' (H_{ac}, T), and (d) imaginary/out-of-phase χ'' (H_{ac}, T) components (solid downward black arrow points toward the peak shift with excitation frequency).

of the ac susceptibility in Fig. 7. In Fig. 7(b), one can clearly observe a decrease in both the amplitude and freezing temperature (T_f) with the increasing excitation frequency, indicating a glassy magnetic state of the sample. Therefore, frequency sensitivity (Mydosh Parameter) of Er_2Cu_2In was estimated to be $\delta T_f = 0.014$, using the formula [1,43]

$$\delta T_f = \frac{\Delta T_f}{T_f(\Delta \log_{10} f)}, \tag{6}$$

where ΔT_f is the change in T_f for a change of the logarithmic excitation frequency($\Delta \log_{10} f$), and T_f is the freezing temperature at the lowest measured excitation frequency of 300 Hz. This value of δT_f falls within the reported range of canonical spin glasses (0.004–0.018) [43]. Consequently, we can conclude that Er_2Cu_2In exhibits properties similar to those of canonical spin glasses [38,44]. Note that δT_f is estimated from the end points; therefore, we subsequently performed a detailed analysis of the ac-susceptibility data. In this context, the frequency dependence of the freezing temperature is further analyzed with the dynamic scaling theory, employing the relation [1,38,43]

$$\tau = \tau_0 \left(\frac{T_f - T_g}{T_g} \right)^{-z\nu}, \tag{7}$$

where τ is the relaxation time corresponding to the measured frequency ($\tau = 1/f$), τ_0 is the characteristic relaxation time for the flipping of single spin entity, T_g is the spin glass/freezing temperature in the limit as frequency approaches zero, and $z\nu$ is the dynamic exponent [see Fig. 8(a)]. The estimated values using Eq. (7) are $\tau_0 = 6.5 \times 10^{-12}$ s, $T_g = 39.1 \pm 0.1$ K, and $z\nu = 4.9 \pm 0.2$. Interestingly, the literature indicates that for canonical spin glasses, τ_0 typically ranges from 10^{-12} to 10^{-14} sec, while $z\nu$ lies between 4 and 12 [43]. Hence, compared to this range, we can conclude that Er_2Cu_2In is a prototype of the canonical spin glass compounds.

Furthermore, the dynamical scaling behavior of spin freezing is extended to the Vogel-Fulcher law with the increased

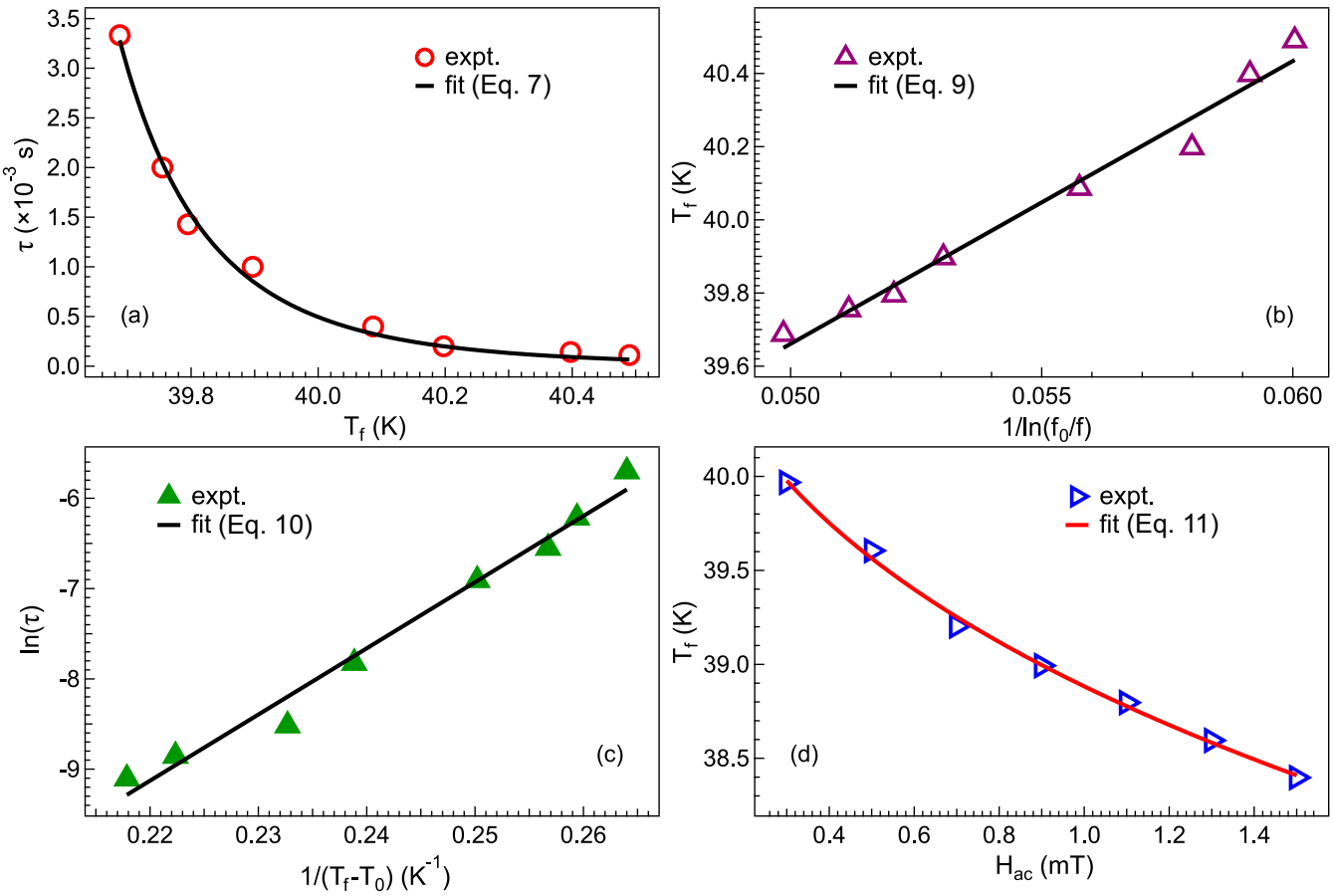


FIG. 8. (a) A power-law fit of spin relaxation time (τ) versus freezing temperature (T_f) using the dynamical scaling law [Eq. (7)], (b) a linear fit is used for the estimation of modified Vogel-Fulcher law keeping τ_0 constant [Eq. (9)], (c) another form of modified Vogel-Fulcher law with T_0 constant with the linear fit [Eq. (10)], and (d) a power-law fit of the freezing temperature for imaginary component of ac susceptibility with the different ac-driven fields [Eq. (11)].

fitting variables using a relation [38,43,45],

$$\tau = \tau_0 \exp\left[\frac{-E_a}{k_B(T_f - T_0)}\right], \tag{8}$$

where T_0 is the characteristic/Vogel-Fulcher temperature utilized to measure the strength of interaction among magnetic entities. The simplified form of the above equation in terms of

$$T_f = \frac{E_a/k_B}{\ln(\tau/\tau_0)} + T_0 \tag{9}$$

is used in Fig. 8(b), demonstrates that a linear fit (solid black line) of the plot between T_f versus $1/\ln(f_0/f)$ results in $E_a/k_B = 77.3 \pm 4.5$, and $T_0 = 35.8 \pm 0.3$ K. The value of E_a/k_B is comparable to previously reported values for the spin glass systems [43], and a higher nonzero value of T_0 indicates an interaction among the magnetic entities. Moreover, to verify these values, we utilized another form of Eq. (8), such that

$$\ln(\tau) = \ln(\tau_0) - \frac{E_a/k_B}{T_f - T_0}. \tag{10}$$

Therefore, we have plotted a graph between $\ln(\tau)$ and $1/(T_f\text{-}T_0)$ in Fig. 8(c), where we have used the value of $T_0 = 35.5 \pm 0.2$ s obtained from the Souletie and Tholence [45] criterion. A linear fit in (solid black line) Fig. 8(c) results in the value of $\tau_0 = 1.1 \times 10^{-11}$ s from the intercept and the $E_a/k_B = 73.3 \pm 4$ is estimated from the slope. These values are in good agreement with the previously obtained values. Therefore, we can conclude that the Eu_2Cu_2In behaves like a canonical spin glass.

Furthermore, the real and the imaginary components of the ac-susceptibility data are measured under different ac-driven fields between 0.3 and 1.5 mT at a constant excitation frequency of 1000 Hz, where from the imaginary component of ac susceptibility in Fig. 8(d), it is evident that with the decreasing ac-driven field, the magnitude of $\chi'(H_{ac}, T)$ is significantly suppressed and shifts to higher temperature from 38.4 to 40.1 K with changing field from 0.3 to 1.5 mT, respectively [highlighted with a solid downward black arrow in Fig. 7(d)]. This variation of T_f can be approximated with the non-mean-field scaling theory in the low-field region using the relation [37]

$$T_f(H_{ac}) = T_0^f\left(1 - A_f H_{ac}^{2/\Phi_f}\right), \tag{11}$$

where A_f is the amplitude for freezing temperature, T_0^f is the value of freezing temperature in the limit of zero ac-magnetic field, and Φ_f is the value of the crossover exponent for freezing temperature on ac-magnetic field. The obtained values of fitting parameters are $A_f = 0.039 \pm 0.002$, $T_0^f = 42.32 \pm 1.05$, and $\Phi_f = 6.29 \pm 2.08$. Interestingly, here, the

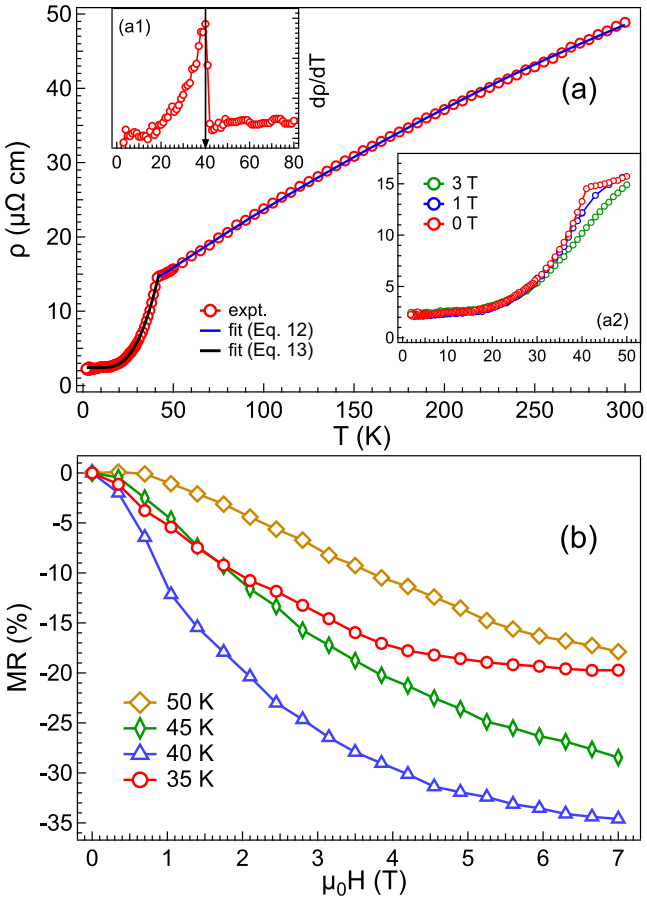


FIG. 9. (a) Temperature dependence of the electrical resistivity [$\rho(T)$] of Er_2Cu_2In along with the fit of $\rho(T)$, above T_C using Eq. (12) (solid blue line) and below T_C using Eq. (13) (solid black line). The top inset (a1) shows the $d\rho/dT$, with the arrow indicating the position of the Curie/transition temperature T_C, and the bottom inset (a2) shows the temperature-dependence of the resistivity at different dc-magnetic fields of 0, 1, and 3 T, and (b) Magnetoresistance of Er_2Cu_2In at constant temperatures of 35, 40, 45, and 50 K.

obtained value of Φ_f is large compared to the defined AT/GT regimes, and it manifests that Er_2Cu_2In diverges from these conventional regimes in the H-T phase space. In addition, the value of Φ_{irr} obtained in Fig. 5(b) is statistically lying in the same range of 4.59 ± 0.45, which is evaluated on the different scales of ac- and dc-magnetic fields. Moreover, similar values of Φ_f are obtained in the literature [38–41,46]. These results manifest that the Er_2Cu_2In compound exhibits a ferromagnetic behavior with the canonical spin glass behavior and diverges from the AT/GT criterion.

E. Electrical resistivity

Figure 9(a) shows the temperature dependence of the electrical resistivity $\rho(T)$ in the absence of an externally applied magnetic field for Er_2Cu_2In. As seen in Fig. 9(a), $\rho(T)$ gradually decreases with decreasing temperatures and shows a sharp drop around T_C. This observed rapid reduction of $\rho(T)$ below 41 K is ascribed to the formation of the ferromagnetic state. Above the transition temperature, $\rho(T)$ gradually increases with increasing temperatures, revealing that the compound exhibits a normal metallic behavior. The almost linear behavior of the $\rho(T)$ in the temperature range of 300 to ~60 K revealed the absence of a crystal electric field effect in the paramagnetic region. Below the transition temperature, the resistivity decreases due to the reduction in the scattering of conduction electrons in the magnetic order state [36]. The top inset (a1) of Fig. 9(a) displays $d\rho(T)/dT$ for the pronounced feature of T_C in $\rho(T)$. According to the criterion of Sato *et al.* [47], the T_C can be defined as a midpoint of the anomaly in the temperature variation $d\rho(T)/dT$ curve. The appearance of a magnetic phase transition in $\rho(T)$ at 41 K [marked by a solid black arrow in the inset (a1) of Fig. 9(a)] is consistent with the results of $\chi(T)$ and $C_p(T)$. Here, $\rho(T)$ was also measured under an externally applied dc-magnetic field of 1 and 3 T, shown in the inset (a2) of Fig. 9(a) with $\rho(T)$ measured at zero dc-magnetic field.

In Fig. 9(a), one can clearly see that above T_C, $\rho(T)$ deviates from an ideal linear metallic behavior and exhibits a curvature. This curvature effect in intermetallic alloys is correlated with the scattering of conduction electrons, the crystal electric field, and strong electron-phonon interaction, as discussed above when evaluating the Hamiltonian. In addition, below T_C, $\rho(T)$ strongly deviates from this behavior owing to the strong interband scattering from $s-d$ interactions. First, we evaluate $\rho(T)$ behavior above T_C, which is fitted using the Bloch-Grüneisen-Mott formula [34,48],

$$\rho(T) = \rho_0 + \frac{4A}{\Theta_D}\left(\frac{T}{\Theta_D}\right)^5 \int_0^{\Theta_D/T} \frac{x^5 dx}{(e^x-1)(1-e^{-x})} - KT^3, \tag{12}$$

where ρ_0 is the residual resistivity, A is the electron-phonon coupling constant, Θ_D is the Debye temperature, and the last term defines $s-d$ interband scattering, and K is the Mott coefficient. The best fit (solid blue line) to Eq. (12) above T_C in Fig. 9(a) between a temperature range of 42–300 K yields $\rho_0 = 2.55(7)\,\mu\Omega\,\text{cm}$, $A = 0.78\,\mu\Omega\,\text{cm K}$, $\Theta_D = 159$ K, and $K = 1.5 \times 10^{-7}\,\mu\Omega\,\text{cm}$. The value of the Mott coefficient (K) for Er_2Cu_2In is sufficiently large compared to similar intermetallic alloys $(Pr/Y)_2Rh_3Ge$ [34] and indicates a higher interband $s-d$ scattering of the conduction electrons.

The magnetic phase transition in χ_{dc}(T), C_p(T), and χ_{ac}(T) as shown in Figs. 2, 4, and 7, respectively, appears close to the $\rho(T)$ in Fig. 9(a). Therefore, this transition is closely related to the magnetic phase transition and spin glass phase of Er_2Cu_2In. To further understand the correlation between the ordered magnetic transition and the resistivity behavior, which possibly leads to the scattering of the conduction electrons on ferromagnetic magnons, as discussed in the Refs. [34,49]. In this line, we fit the zero-field $\rho(T)$ in Fig. 9(a) using the equation [49]

$$\rho_{SW}(T) = \rho_0^{FM} + A^{FM} T \Delta_\rho \exp\left(\frac{2T}{\Delta_\rho}\right) \times \left[1 + \frac{2T}{\Delta_\rho} + \frac{1}{2}\exp\left(\frac{2T}{\Delta_\rho}\right)\right]. \tag{13}$$

Here, $\rho_{SW}(T)$, ρ_0^{FM}, A^{FM}, and Δ_ρ are the resistivity showing the scattering of conduction electrons due to FM

magnons (spin wave resistivity), residual resistivity of the ordered magnetic state, material constant depends on the spin wave stiffness, and energy gap in the FM magnon spectrum, respectively. A best fit (solid black line) of $\rho(T)$ to Eq. (13) between the temperature range of 1.8 and 41 K yields $\rho_0^{\mathrm{FM}} = 2.32(2)\,\mu\Omega\,\mathrm{cm}$, $A^{\mathrm{FM}} = 9.62(6) \times 10^{-9}\,\Omega\,\mathrm{cm}$, and $\Delta_\rho = 70.25 \pm 0.27$ K. The value of $\Delta_\rho = 70.25 \pm 0.27$ K, equal to 6.05 ± 0.02 meV, is very close to the other reported values of magnon gaps in the fundamental Shashtry-Sutherland lattice of 5 meV, perovskite $SrRuO_3$ of 35 meV ($T_C \approx 165$ K) [50], helimagnet FeP with a gap of 5 meV [51], and in bilayer compound $Sr_3Ir_2O_7$ the giant magnon gap of 92 meV is observed [52].

The observed $\rho(T)$ with applied magnetic field gets broadened, and the anomaly is not discernible around T_C. This feature is commonly seen in ferromagnetically ordered systems [34]. The magnetoresistance (MR) was estimated from the field dependence of electrical resistivity using the following relation,

$$\mathrm{MR} = \frac{\rho(\mathrm{H,T}) - \rho(0,\mathrm{T})}{\rho(0,\mathrm{T})} \times 100\%, \tag{14}$$

where $\rho(0, T)$ is the resistivity at zero magnetic field and $\rho(H, T)$ is the resistivity at applied magnetic field. The obtained field dependence of MR for different temperatures near the transition region is shown in Fig. 9(b). One can see from this figure that the magnitude of MR is negative over a wide temperature range. MR reaches a maximum value of ≈35% at 40 K (near $T_C = 41$ K) for a magnetic field of 7 T. The MR value of 35% appears to be the largest reported among various R_2T_2X compounds.

IV. CONCLUSIONS

In conclusion, the investigation of Er_2Cu_2In reveals its interesting magnetic behavior and distinctive characteristics. The compound forms a tetragonal crystal structure and undergoes a second-order ferromagnetic phase transition with $T_C = 41$ K, with ferromagnetic exchange interactions indicated by a positive Curie-Weiss temperature. The magnetization measurements show magnetic anisotropy and crystal field effects in our polycrystalline sample Er_2Cu_2In. The compound exhibits a λ-shaped anomaly in specific heat capacity, indicating a second-order ferromagnetic transition. Below T_C, the C_P data is well described considering an FM spin wave spectrum with an energy gap of 37 K. The $\rho(T)$ result suggests that Er_2Cu_2In is an ordinary metal in its paramagnetic state and exhibits a large negative magnetoresistance around T_C. The Eu_2Cu_2In's temperature-dependent dc magnetization and ac susceptibility reveal spin glass behavior below T_C. The shift in ac susceptibility at the spin glass transition temperature indicates geometric/magnetic frustration. The dynamic scaling theory and Vogel-Fulcher law suggest the presence of spin freezing and interactions between magnetic entities. The TRM analysis reveals complex spin dynamics and relaxation processes similar to those observed in metallic glasses. Overall, Er_2Cu_2In exhibits spin glass behavior with large magnetoresistance, highlighting its intricate magnetic properties. The results of our study pave the way for further investigations into the interesting magnetic behavior of Er_2Cu_2In, and especially on single-crystal material to search for connections at the confluence of magnetic anisotropy, geometric frustration, and ferromagnetic ordering that also involves spin glass freezing.

ACKNOWLEDGMENTS

R.D.F. thanks OWSD and SIDA for the fellowship towards Ph.D. studies. A.M.S. thanks the URC/FRC of UJ for the financial support.

DATA AVAILABILITY

The data that support the findings of this article are not publicly available. The data are available from the authors upon reasonable request.

[1] J. A. Mydosh, *Spin Glasses: An Experimental Introduction* (CRC Press, London, 1993).

[2] M. Mézard, G. Parisi, and M. A. Virasoro, *Spin Glass Theory and Beyond: An Introduction to the Replica Method and Its Applications* (World Scientific Publishing Company, Singapore, 1987), Vol. 9.

[3] K. Binder and A. P. Young, Spin glasses: Experimental facts, theoretical concepts, and open questions, Rev. Mod. Phys. **58**, 801 (1986).

[4] M. Gabay and G. Toulouse, Coexistence of spin-glass and ferromagnetic orderings, Phys. Rev. Lett. **47**, 201 (1981).

[5] V. K. Anand, D. T. Adroja, and A. D. Hillier, Ferromagnetic cluster spin-glass behavior in $PrRhSn_3$, Phys. Rev. B **85**, 014418 (2012).

[6] V. K. Anand, D. T. Adroja, A. D. Hillier, J. Taylor, and G. André, Signatures of spin-glass behavior in the induced magnetic moment system $PrRuSi_3$, Phys. Rev. B **84**, 064440 (2011).

[7] A. Krimmel, J. Hemberger, M. Nicklas, G. Knebel, W. Trinkl, M. Brando, V. Fritsch, A. Loidl, and E. Ressouche, Spin-glass behavior in $PrAu_2Si_2$, Phys. Rev. B **59**, R6604 (1999).

[8] E. A. Goremychkin, R. Osborn, B. D. Rainford, R. T. Macaluso, D. T. Adroja, and M. Koza, Spin-glass order induced by dynamic frustration, Nat. Phys. **4**, 766 (2008).

[9] T. C. Ozawa, T. Taniguchi, Y. Kawaji, Y. Nagata, Y. Noro, H. Samata, and S. Takayanagi, Spin frustration and antiferromagnetic long-range order in R_2BaPdO_5 (R = rare earth), Phys. Lett. A **337**, 130 (2005).

[10] J. Y. Lee, Y. You, S. Sachdev, and A. Vishwanath, Signatures of a deconfined phase transition on the Shastry-Sutherland lattice: Applications to quantum critical $SrCu_2(BO_3)_2$, Phys. Rev. X **9**, 041037 (2019).

[11] B. S. Shastry and B. Sutherland, Exact ground state of a quantum mechanical antiferromagnet, Physica B+C **108**, 1069 (1981).

[12] J. G. Sereni, Comparison of a Shastry-Sutherland lattice stability in Ce_2Pd_2Sn as a function of field and doping, J. Phys.: Conf. Ser. **273**, 012126 (2011).

[13] J. G. Sereni, J. Roberts, F. Gastaldo, M. G–Berisso, and M. Giovannini, Shastry–Sutherland phase formation in magnetically frustrated $Ce_2Pd_2In_{1-x}Sn_x$ alloys, Mater. Today: Proc. **14**, 80 (2019).

[14] K. Iwakawa, Y. Hirose, K. Enoki, K. Sugiyama, T. Takeuchi, F. Honda, M. Hagiwara, K. Kindo, T. Nakano, Y. Nozue, R. Settai, and Y. Onuki, Multiple metamagnetic transitions in antiferromagnet Yb_2Pt_2Pb with the Shastry–Sutherland lattice, J. Phys. Soc. Jpn. **81**, SB058 (2012).

[15] B. Sahu, R. D. Fobasso, and A. M. Strydom, Spinglass behavior in Shastry–Sutherland lattice of Tm_2Cu_2In, J. Magn. Magn. Mater. **543**, 168599 (2022).

[16] P. Král, M. Diviš, L. Havela, P. Doležal, J. Kaštil, and J. Prchal, Glassy magnetism of Tm_2Cu_2In in elevated pressures, J. Magn. Magn. Mater. **570**, 170527 (2023).

[17] P. Fischer, T. Herrmannsdörfer, T. Bonelli, F. Fauth, L. Keller, E. Bauer, and M. Giovannini, Antiferromagnetic rare-earth ordering in the intermetallic compounds R_2Pd_2In (R = Pr, Nd), J. Phys.: Condens. Matter **12**, 7089 (2000).

[18] S. Maskova-Cerna, M. Klicpera, P. Svoboda, A. V. Andreev, Y. Skourski, M. Reehuis, J. Hoffmann, G. André, and L. Havela, New type of magnetic structure in the R_2T_2X group: Tb_2Pd_2In, J. Phys.: Condens. Matter **32**, 345801 (2020).

[19] Y. Zhang, Review of the structural, magnetic and magnetocaloric properties in ternary rare earth RE_2T_2X type intermetallic compounds, J. Alloys Compd. **787**, 1173 (2019).

[20] A. Doğan, S. Rayaprol, and R. Pöttgen, New Mo_2FeB_2 type intermetallic cadmium compounds RE_2Pd_2Cd (RE = Pr, Sm, Gd–Lu)–synthesis, structure, and magnetic properties, J. Phys.: Condens. Matter **19**, 026209 (2007).

[21] T. Fickenscher, U. C. Rodewald, D. Niepmann, R. Mishra, M. Eschen, and R. Pöttgen, The Mo_2FeB_2- and Mn_2AlB_2-type modifications of RE_2Ni_2Cd (RE = La, Pr, Nd, Sm, Tb, Dy), Z. Naturforsch. B **60**, 271 (2005).

[22] F. M. Schappacher, W. Hermes, and R. Pöttgen, Structure and magnetic properties of RE_2Cu_2Cd, J. Solid State Chem. **182**, 265 (2009).

[23] I. R. Fisher, Z. Islam, and P. C. Canfield, Magnetic and transport properties of single-crystal R_2Cu_2In (R = Gd–Tm, Lu), J. Magn. Magn. Mater. **202**, 1 (1999).

[24] K. A. Miliyanchuk, V. Kolomiets, Y. V. Galadzhun, L. Havela, I. I. Bulyk, A. M. Trostianchyn, and Y. M. Kalychak, Structure and magnetism of new R_2Cu_2In hydrides (R = Ce, Gd), Chem. Met. Alloys **1**, 46 (2008).

[25] S. Rayaprol and R. Pöttgen, Gd_2Au_2Cd: A Mo_2FeB_2-type intermetallic with ferromagnetic ordering and spin glass anomalies, Phys. Rev. B **73**, 214403 (2006).

[26] G. Sala, M. Stone, and A. Christianson, Frustrated magnetism on Nd–based Shastry-Sutherland (SS) lattices, Acta Cryst. **A75**, a226 (2019).

[27] H. M. Rietveld, A profile refinement method for nuclear and magnetic structures, J. Appl. Cryst. **2**, 65 (1969).

[28] Juan Rodriguez-Carvajal, Recent advances in magnetic structure determination by neutron powder diffraction, Phys. B: Condens. Matter **192**, 55 (1993).

[29] Y. Zhang, Y. Yang, X. Xu, L. Hou, Z. Ren, X. Li, and G. Wilde, Large reversible magnetocaloric effect in RE_2Cu_2In (RE = Er and Tm) and enhanced refrigerant capacity in its composite materials, J. Phys. D: Appl. Phys. **49**, 145002 (2016).

[30] K. Momma and F. Izumi, *VESTA 3* for three-dimensional visualization of crystal, volumetric and morphology data, J. Appl. Cryst. **44**, 1272 (2011).

[31] S. Pakhira, C. Mazumdar, R. Ranganathan, S. Giri, and M. Avdeev, Large magnetic cooling power involving frustrated antiferromagnetic spin-glass state in R_2NiSi_3 (R = Gd, Er), Phys. Rev. B **94**, 104414 (2016).

[32] A. Scheie, *PyCrystalField*: software for calculation, analysis, and fitting of crystal electric field Hamiltonians, J. Appl. Cryst. **54**, 356 (2021).

[33] See Supplemental Material at http://link.aps.org/supplemental/10.1103/jqs4-hg41 for computational details of magnetic exchange constants (J_{ij}) and Dzyaloshinskii-Moriya interactions (D_{ij}).

[34] M. Falkowski and A. M. Strydom, A new ternary magnetically ordered heavy fermion compound Pr_2Rh_3Ge: magnetic, electronic and thermodynamic properties, J. Phys.: Condens. Matter **29**, 395601 (2017).

[35] A. Tari, *The Specific Heat of Matter at Low Temperatures* (Imperial College Press, London, 2003).

[36] M. T. Tchokonté, J. J. Mboukam, A. K. H. Bashir, B. M. Sondezi, K. Ramesh Kumar, A. M. Strydom, and D. Kaczorowski, Electrical resistivity and thermodynamic properties of the ferromagnet Nd_2Pt_2In, J. Alloys Compd. **753**, 41 (2018).

[37] J. R. L. de Almeida and D. J. Thouless, Stability of the Sherrington-Kirkpatrick solution of a spin glass model, J. Phys. A: Math. Gen. **11**, 983 (1978).

[38] P. Bag, P. R. Baral, and R. Nath, Cluster spin-glass behavior and memory effect in $Cr_{0.5}Fe_{0.5}Ga$, Phys. Rev. B **98**, 144436 (2018).

[39] T. J. Bullard, M. A. Susner, K. M. Taddei, J. A. Brant, and T. J. Haugan, Magnetic and structural properties of the solid solution $CuAl_{2(1-x)}Ga_{2x}O_4$, Sci. Rep. **11**, 11355 (2021).

[40] B. Barbara, A. P. Malozemoff, and Y. Imry, Scaling of nonlinear susceptibility in MnCu and GdAl spin-glasses, Phys. Rev. Lett. **47**, 1852 (1981).

[41] B. Dieny and B. Barbara, Critical properties of a random-anisotropy system a-DyNi: A new universality class in disordered systems? Phys. Rev. Lett. **57**, 1169 (1986).

[42] Q. Luo, D. Q. Zhao, M. X. Pan, and W. H. Wang, Critical and slow dynamics in a bulk metallic glass exhibiting strong random magnetic anisotropy, Appl. Phys. Lett. **92**, 011923 (2008).

[43] R. Shukla, A. Jain, M. Miryala, K. Ueno, M. Murakami, S. M. Yusuf, and R. S. Dhaka, Spin dynamics and Unconventional Magnetism in Insulating $La_{1-2x}Sr_{2x}Co_{1-x}Nb_xO_3$, J. Phys. Chem. C **123**, 22457 (2019).

[44] Y. Bitla, S. N. Kaul, and L. F. Barquín, Nonlinear susceptibilities as a probe to unambiguously distinguish between canonical and cluster spin glasses, Phys. Rev. B **86**, 094405 (2012).

[45] J. Souletie and J. L. Tholence, Critical slowing down in spin glasses and other glasses: Fulcher versus power law, Phys. Rev. B **32**, 516 (1985).

[46] P. M. Shand, T. Rash, M. Streicher, T. E. Kidd, K. R. Boyle, and L. H. Strauss, Coercivity and exchange bias of $Mn_{0.25}Ti_{1.1}S_2$ in the cluster-glass state, Phys. Rev. B **82**, 214413 (2010).

[47] N. Sato, N. Aso, K. Hirota, T. Komatsubara, Y. Endoh, S. M. Shapiro, G. H. Lander, and K. Kakurai, Anisotropy and two

length scales in the magnetic critical scattering in the heavy-fermion superconductor UPd_2Al_3, Phys. Rev. B **53**, 14043 (1996).

[48] N. F. Mott and H. Jones, *The Theory of the Properties of Metals and Alloys* (Oxford University Press, London, 1958).

[49] N. H. Andersen and H. Smith, Electron-magnon interaction and the electrical resistivity of Tb, Phys. Rev. B **19**, 384 (1979).

[50] K. Jenni, S. Kunkemöller, A. Tewari, R. A. Ewings, Y. Sidis, A. Schneidewind, P. Steffens, A. A. Nugroho, and M. Braden, Magnon dispersion in ferromagnetic $SrRuO_3$, Phys. Rev. B **107**, 174429 (2023).

[51] A. S. Sukhanov, Y. V. Tymoshenko, A. A. Kulbakov, A. S. Cameron, V. Kocsis, H. C. Walker, A. Ivanov, J. T. Park, V. Pomjakushin, S. E. Nikitin, I. V. Morozov, I. O. Chernyavskii, S. Aswartham, A. U. B. Wolter, A. Yaresko, B. Büchner, and D. S. Inosov, Frustration model and spin excitations in the helimagnet FeP, Phys. Rev. B **105**, 134424 (2022).

[52] J. Kim, A. H. Said, D. Casa, M. H. Upton, T. Gog, M. Daghofer, G. Jackeli, J. van den Brink, G. Khaliullin, and B. J. Kim, Large spin-wave energy gap in the bilayer iridate $Sr_3Ir_2O_7$: Evidence for enhanced dipolar interactions near the Mott metal-insulator transition, Phys. Rev. Lett. **109**, 157402 (2012).